Article

Facile Fabrication of a Selective Poly(caffeic acid)@MWCNT-Ni(OH)$_2$ Hybrid Nanomaterial and Its Application as a Non-Enzymatic Glucose Sensor

Maria Kuznowicz [1], Tomasz Rębiś [2], Artur Jędrzak [1,3], Grzegorz Nowaczyk [3] and Teofil Jesionowski [1,*]

[1] Institute of Chemical Technology and Engineering, Faculty of Chemical Technology, Poznan University of Technology, Berdychowo 4, PL-60965 Poznan, Poland

[2] Institute of Chemistry and Technical Electrochemistry, Faculty of Chemical Technology, Poznan University of Technology, Berdychowo 4, PL-60965 Poznan, Poland; tomasz.rebis@put.poznan.pl

[3] NanoBioMedical Centre, Adam Mickiewicz University, Wszechnicy Piastowskiej 3, PL-61614 Poznan, Poland

* Correspondence: teofil.jesionowski@put.poznan.pl

Abstract: A novel catechol-based PCA@MWCNT-Ni(OH)$_2$ hybrid material was prepared and used to construct a non-enzymatic glucose biosensor. In this synthesis, MWCNTs were covered with a poly(caffeic acid) coating and then subjected to a straightforward electrochemical process to decorate the hybrid material with Ni(OH)$_2$ particles. The physicochemical properties and morphology of the nanomaterial were characterized using high-resolution transmission electron microscopy (HRTEM), X-ray photoelectron spectroscopy (XPS), energy-dispersive X-ray spectroscopy (EDS), and atomic force microscopy (AFM). Amperometry and cyclic voltammetric studies demonstrated the enhanced redox properties of a GC/PCA@MWCNT-Ni(OH)$_2$ electrode and its electrocatalytic activity in glucose detection, with a low detection limit (0.29 μM), a selectivity of 232.7 μA mM^{-1} cm^{-2}, and a linear range of 0.05–10 mM, with good stability (5 months) and reproducibility ($n = 8$). The non-enzymatic sensor was also used for glucose determination in human serum and human blood, with recovery values ranging from 93.3% to 98.2%. In view of the properties demonstrated, the described GC/PCA@MWCNT-Ni(OH)$_2$ sensor represents a facile synthesis method of obtaining the hybrid nanomaterial and a low-cost approach to electrochemical glucose measurement in real samples (human serum, human blood).

Keywords: glucose electrochemical sensor; non-enzymatic sensor; poly(caffeic acid); nickel oxide nanoparticles

1. Introduction

Glucose detection and monitoring are currently of great importance, especially in the food industry and in the treatment of diabetes [1,2]. Millions of people worldwide are affected by diabetes, which is ranked as the third most common chronic incurable disease and the prevalence of which is steadily increasing [3]. It typically results from a rise in the amount of sugar in bodily fluids, including blood, tears, urine, and serum, which can lead to problems with the heart, kidneys, sight, etc. Only effective therapies and regular diagnostics will prevent this. Due to the fact that the traditional method of diagnostic glucose measurement is time-consuming and expensive, a current aim is to create a low-cost, fast, and reliable glucose sensor with excellent selectivity and sensitivity [4].

In prior research, non-enzymatic glucose sensors have been constructed using various transition materials and metal oxides [5–8]. Non-enzymatic electrochemical sensors for the detection of various biomolecules have gained much interest due to their direct electrocatalytic detection method, cost-effective construction, excellent stability, and repeatability [9]. Glucose oxidation can be achieved using electrodes based on Ni, NiO, or Ni(OH)$_2$ due

to the presence of the redox pair $Ni(OH)_2/NiOOH$, which is formed in an alkaline environment on the surface of the electrode [10]. Nickel(II) hydroxide is one of the relatively low-cost materials that can be used in effective electrocatalysts for glucose detection. Enzymatic and non-enzymatic glucose sensors already have new application platforms due to recent advancements in nanomaterial production [11]. Moreover, the use of nanostructured materials can considerably increase the activity of $Ni(OH)_2$ electrodes [12].

Various materials using the $Ni(OH)_2/NiOOH$ mechanism for glucose sensing have recently been reported. They enable the low-cost production of electrochemical sensors, taking advantage of the catalytic abilities of nickel. Gao et al. proposed a non-enzymatic glucose sensor based on nickel(II) hydroxide/electro-reduced graphene oxide ($Ni(OH)_2/ERGO$) nanocomposites with multi-walled carbon nanotubes (MWCNTs). They applied a simple method of synthesis in line with the principles of green chemistry and demonstrated the good electrocatalytic effect of $Ni(OH)_2$ nanoparticles in detecting glucose. The proposed system enabled the detection of glucose in a range of 10 μM to 9050 μM, with an LOD of 4.0 μM. Moreover, Gao et al. used the proposed sensor for testing with real samples [13]. In our previous work, we presented a hybrid nanomaterial poly(caffeic acid)@MWCNT (PCA@MWCNT) characterized by the presence of peaks from the functional groups contained in the biopolymer—PCA coating. This made it possible to lower the potential at which NADH measurements were carried out, thus minimizing the influences of interfering agents on the measurements [14]. The obtained results were then used for the construction of a non-enzymatic glucose sensor by decorating the PCA@MWCNT nanomaterial with CuO. This made it possible to obtain a non-enzymatic glucose sensor with a sensitivity of 2412 μA mM^{-1} cm^{-2}, a detection limit of 0.43 μM, and a linearity range of 0.002–9.0 mM [8].

In this work, we present a simple method to create a PCA@MWCNT hybrid nanomaterial and electrochemically decorate it with $Ni(OH)_2$. The novelty of the proposed sensor consists of the use of a PCA functional biomimetic polymer, in accordance with the principles of green chemistry, and its combination with a nickel compound that enables glucose detection. The PCA@MWCNT-$Ni(OH)_2$ material was characterized in detail using several physicochemical techniques. In addition, it was used to build a non-enzymatic glucose sensor. The experimental results showed good sensitivity and selectivity over other compounds that occur in human blood and may be interfering factors. In addition, the sensor was tested in real solutions (blood, serum), achieving a relatively high recovery. Therefore, the proposed non-enzymatic sensor may be an alternative practical method for the detection of glucose levels in real samples. The proposed system demonstrated high recovery for measurements in real solutions such as human blood and human serum, with simultaneous long stability of the sensor over time (5 months).

2. Materials and Methods

2.1. Materials and Chemicals

Caffeic acid (CA), nickel(II) sulfate hexahydrate, glucose, L-cysteine, dopamine, ascorbic acid, uric acid, fructose, maltose, saccharose, potassium hexacyanoferrate(II) trihydrate, potassium hexacyanoferrate(III), dipotassium hydrogen phosphate, potassium dihydrogen phosphate, and human serum samples (from human male AB plasma) were purchased from Merck. Multi-walled carbon nanotubes (MWCNTs) were obtained from DropSens (average diameter: ca. 10 nm, average length: 1–2 μm). Sodium hydroxide was purchased from POCH Gliwice. Meter TraxTM Control whole blood samples with various low*, medium*, and high* concentrations of glucose (*company markings) were supplied by Bio-Rad.

2.2. Apparatus

A μ-Autolab III potentiostat (ECO Chemie, Netherlands) was used for the electrode-position of nickel oxide and for all electrochemical measurements. The reference electrode was Ag/AgCl/3M KCl, and Pt wire was used as the counter electrode. The working

electrode was a glassy carbon electrode (GC; d = 2 mm). XPS analysis was conducted with the use of a Prevac UHV multi-chamber analytical system. The radiation source was a VG Scienta SAX 100 X-ray lamp with an aluminum anode, equipped with a VG Scienta XM 780 monochromator and emitting radiation with the Al Kα characteristic line and energy of 1486.7 eV. High-resolution transmission electron microscopy (HRTEM) was performed with a maximum acceleration of 120 kV and a resolution of 2 nm, with analysis using a Jeol ARM 200F instrument. AFM measurements were performed under ambient conditions using a Park NX10 microscope in intermittent contact mode.

2.3. Fabrication of GC/PCA@MWCNT-Ni(OH)$_2$ Nanoplatform

Synthesis of the PCA@MWCNT material was performed as described in our previous work [8]. To obtain a PCA@MWCNT hybrid material, 10 mg of caffeic acid (CA; 5.6 mM) was dispersed in 10 mL of deionized water, and then 10 mg of MWCNT was added. The mixture was next sonicated for 20 min to obtain a homogeneous solution, and a prepared solution of NaIO$_4$ (12 mg dissolved in 10 mL; 4.7 mM) was added dropwise. The process was allowed to take place for 24 h, after which the solution was washed with a water/methanol mixture (20 min; 6000 rpm).

Before the electrodecoration of the PCA@MWCNT hybrid material with Ni(OH)$_2$, the GC electrode was polished with Al$_2$O$_3$ (Buehler; average diameter: 50 nm) on a polishing cloth. It was then rinsed with a water/acetone mixture (1:1) in an ultrasonic bath.

To decorate the electrode with nickel(II) hydroxide, in the first step, the electrode was modified with the PCA@MWCNT hybrid material. Then the modified electrode was immersed in a NiSO$_4$ solution to accumulate Ni^{2+}. To optimize the electrodeposition process, different concentrations of NiSO$_4$ (0.001 to 0.1 M) and immersion times in the solution (from 0.2 to 10 min) were tested (Section 3.1).

2.4. Real Sample Analysis

The standard addition technique was used to measure glucose in real samples (human serum, human blood). For this, each real sample was added to 0.1 M NaOH, followed by the addition of known glucose concentrations. The measurement was carried out using the amperometric I–t relationship. In the case of human serum, three glucose concentrations (2.4, 6.6, and 8.5 mM) were measured. The analysis of the Meter Trax™ Control human whole blood samples consisted of three measurements with different glucose concentrations (3.2, 6.3, and 14.7 mM).

3. Results and Discussion

3.1. Electrochemical Formation of GC/PCA@MWCNT-Ni(OH)$_2$

Our previous studies have shown that the CV response for PCA@MWCNT in PBS (pH = 7.4) exhibits two reversible redox pairs, at E0′ = 0.18 and −0.10 V, related to cross-linked o-quinone/o-hydroquinone transitions [8]. The formation of a coordinating connection between metal ions and deprotonated catechol (quinoid) moieties was discovered in a previous study of the chemical interactions between phenolics and transition metal ions such as copper, iron, and nickel [13]. The catechol groups present in the PCA structure have the potential to function as chelating agents for nickel ions. Furthermore, the functionalization of the GC/PCA@MWCNT electrode with nickel ions was performed in the first step by dipping the modified electrode in an aqueous NiSO$_4$ solution for the required amount of time. As a result, the formation of a Ni^{2+} complex on the surface of the electrode took place according to this equation:

$$GC/PCA@MWCNT + Ni^{2+} \rightarrow GC/PCA@MWCNT\text{-}Ni^{2+} \tag{1}$$
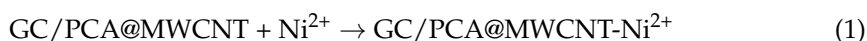
After the Ni^{2+} accumulation, the GC/PCA@MWCNT-Ni^{2+} electrode was transferred to a sodium hydroxide solution (NaOH, 0.1 M). In this solution, the uniformly distributed

nickel centers (Ni^{2+}) on the surface of GC/PCA@MWCNT turned into nanoparticles of $Ni(OH)_2$. The changes can be expressed with this equation:

$$GC/PCA@MWCNT\text{-}Ni^{2+} + 2OH^- \rightarrow GC/PCA@MWCNT\text{-}Ni(OH)_2 \qquad (2)$$

Finally, CVs were recorded in the potential range of 0.0 to +0.6 V in 0.1 M NaOH until reproducible voltammetric signals were obtained. Figure 1 shows the recorded curves. The CVs display a distinct redox couple at $E0' = 0.48$ V. These peaks are due to the oxidation of $Ni(OH)_2$ to NiOOH, which caused the Ni oxidation state to transition from Ni^{2+} to Ni^{3+} according to this equation:

$$GC/PCA@MWCNT\text{-}Ni(OH)_2 + OH^- \leftrightarrow GC/PCA@MWCNT\text{-}NiOOH + H_2O + e^- \quad (3)$$

Similar values of the oxidation potential of $Ni(OH)_2$ have been reported by Liu et al, among others. The proposed $MWCNT/Ni(OH)_2$ system produced an oxidation peak at 0.47 V [14]. Moreover, the $Ni(OH)_2$ was shown by Liu et al. to produce an oxidation peak at 0.48 V, which confirmed the effective deposition of $Ni(OH)_2$ on the present MWCNT@PCA hybrid material [15].

The results we obtained confirm that a surface-confined complex was formed between the catechol groups of PCA and nickel, the ions of which may be a precursor for the in situ creation of nickel hydroxide nanoparticles.
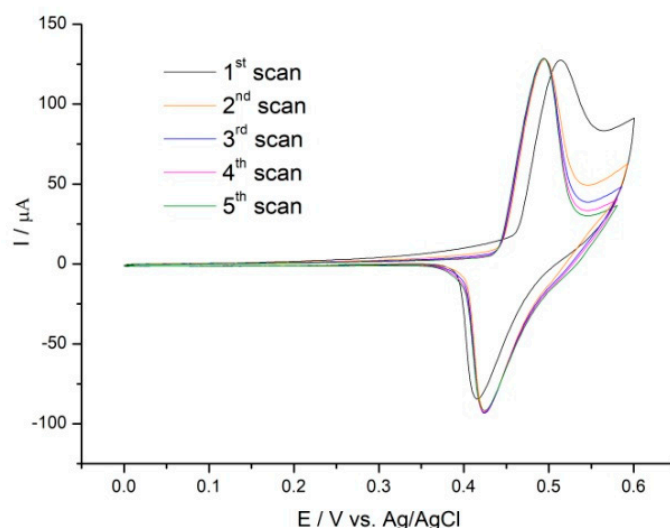

Figure 1. CVs of GC/PCA@MWCNT-Ni in 0.1 M NaOH solution at 10 mV s^{-1}.

3.2. Surface Characterization

High-resolution transmission electron microscopy (HRTEM) was performed to investigate the morphology of the $PCA@MWCNT\text{-}Ni(OH)_2$ nanomaterial. The HRTEM image (Figure 2A) shows the surface MWCNTs covered with a thin poly(caffeic acid) film, with diameters in the range of 3–4 nm, and $Ni(OH)_2$ nanoparticles decorating the surface of the PCA@MWCNT hybrid material. In certain areas, aggregated nanoparticles are visible.

Atomic force microscopy (AFM) was used to determine the morphology of PCA@MWCNT-$Ni(OH)_2$. Figure 2B,C show, respectively, 2D and 3D images of the $Ni(OH)_2$ nanoparticles deposited on the PCA@MWCNT hybrid material. The $Ni(OH)_2$ was electrodeposited mainly at the ends of the carbon nanotubes, which is explained by the accumulation of Ni^{2+} ions in the boundary plane defects, as has been confirmed in previous studies [8]. Moreover, the height profile was determined; this is presented in Figure S1 (see Supplementary Materials). Moreover, based on the determined AFM, an RMS roughness (Sq) value of 208.3 nm was determined.
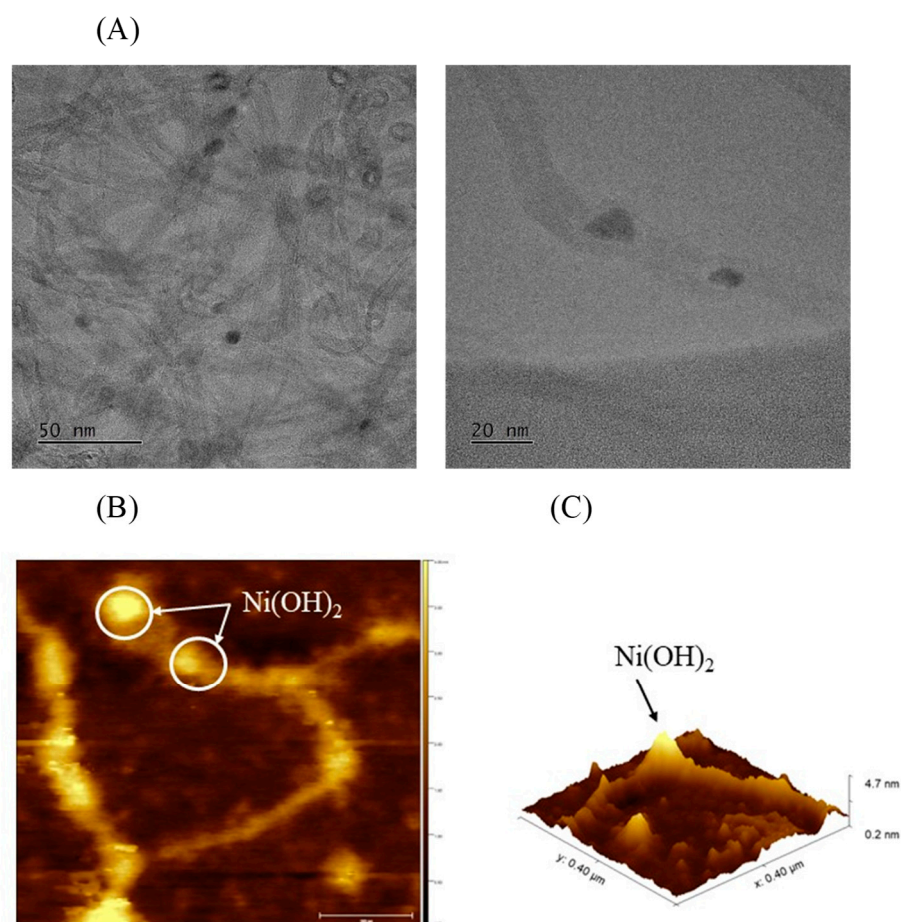
(A)

(B)

(C)

Figure 2. HRTEM images of PCA@MWCNT-Ni(OH)$_2$ at different magnifications (**A**). AFM images of PCA@MWCNT-Ni(OH)$_2$ (**B**,**C**).

The deposition of the Ni(OH)$_2$ on the PCA@MWCNT hybrid material was confirmed with energy-dispersive X-ray spectroscopy (EDS). The EDS mappings of the material were obtained to analyze the elemental distributions of the product surface. Figure S2A shows strong diffraction peaks for C, O, and Ni. The molar ratio of C, O, and Ni was 69.76: 26.46: 3.78, respectively (Table S1). The EDS mapping of the individual elements (Figure S2B–D) shows the uniform distribution of the elements in the sample. Moreover, high homogeneity can be observed, with no identified agglomeration.

Through analysis of X-ray photoelectron spectra (XPSs), the chemical valence and elemental composition of the MWCNT@PCA-Ni(OH)$_2$ hybrid material were confirmed (Figure 3A). According to the survey spectrum, the elements C, Ni, and O coexisted. This is in line with the findings based on the EDS mapping.

In accordance with the graphitic structure and carbon–carbon bonding (C–C and C=C), the XPS for C 1s contained a peak with a binding energy of 284.9 eV (Figure 3B) [16]. The C 1s spectrum of MWCNT@PCA-Ni(OH)$_2$ has also contained peaks attributed to C=O carbonyl groups (287.5 eV) and O=C–O carboxyl groups (288.7 eV) [17].

In the analysis of the O 1s core line (Figure 3C), the presence of –OH bonds was reflected by a peak with a binding energy of 531.5 eV [18]. The peak at 532.8 eV could be attributed to oxygen species in the carboxyl group (C=O). Other components corresponded to oxygen–metal (Ni–O) bonds (530.8 eV) [19] and residual H$_2$O (535.1 eV) [20].

The XPS spectra for the Ni 2p core level recorded in the range of 850–890 eV are shown in Figure 3D. As indicated in the graph, the spectra consisted of two spin-orbit doublets, which correspond to Ni^{2+} and Ni^{3+}, and two shaking satellites. The binding energy of Ni 2p$^{3/2}$ is approximately 856.4 eV, which corresponds to previously reported values [21].
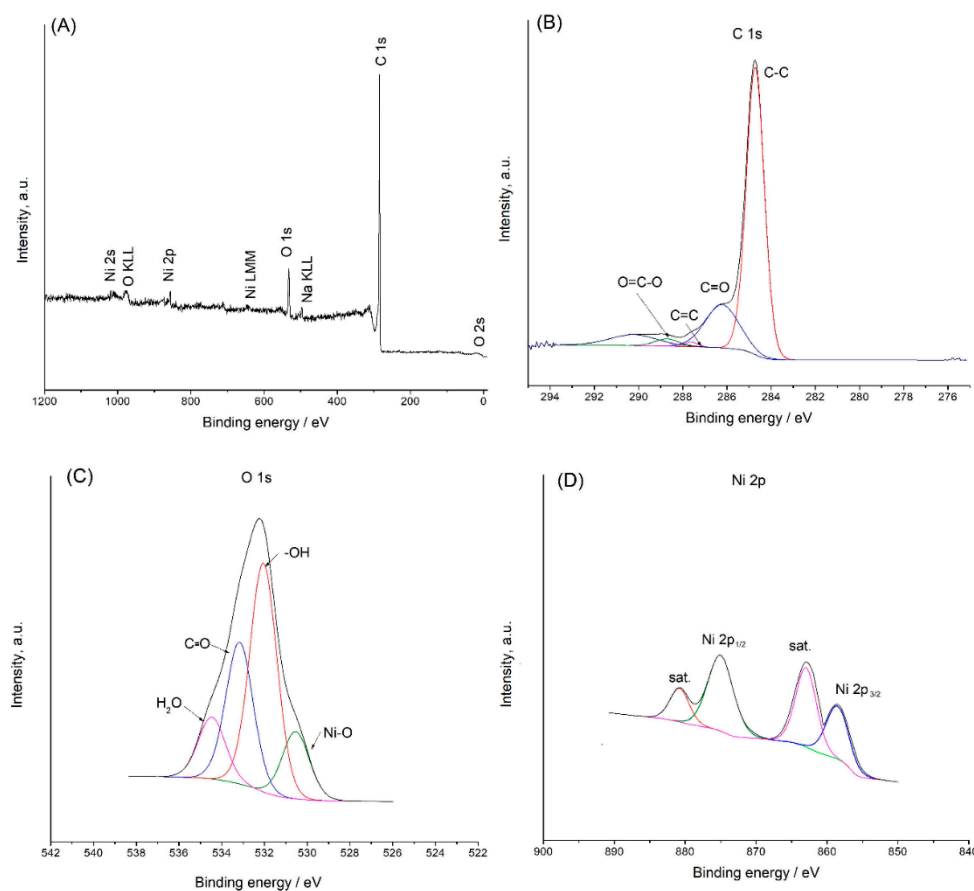
Figure 3. Survey spectrum of the PCA@MWCNT-Ni(OH)$_2$ hybrid material (**A**); XPS results for carbon 1s (**B**), oxygen 1s, and (**C**); nickel 2p (**D**).

3.3. Electrochemical Characterization

The electron transfer ability of the GC/PCA@MWCNT-Ni(OH)$_2$ electrode was assessed with a cyclic voltammetry method using 1 mM of a $[Fe(CN)_6]^{3-/4-}$ solution. For the bare GC electrode (Figure 4A, curve a), a peak separation of 89 mV was observed, indicating the quasi-reversible behavior of the $[Fe(CN)_6]^{3-/4-}$ with bare GC. On the GC/PCA@MWCNT electrode (Figure 4A, curve b), a smaller peak-to-peak separation of 80 mV was obtained. These results are due to the faster electron transfer rate on the highly conductive MWCNT surface than on the bare GC. However, the peak-to-peak separation of 80 mV on the GC/PCA@MWCNT was still larger than expected for the diffusion-controlled reversible redox process ($\Delta E = 60$ mV) [22]. This may have been due to repulsive coulombic interactions between the negatively charged $[Fe(CN)_6]^{3-/4-}$ marker and the carboxylic functional groups of the PCA. The redox response for the GC/PCA@MWCNT-Ni(OH)$_2$ system showed higher peak current values than that for the GC/PCA@MWCNT, while the peak-to-peak separation decreased slightly to 0.79 V (Figure 4A, curve c).

Figure 4B shows the results obtained using electrochemical impedance spectroscopy (EIS) to characterize heterogeneous electron transfer on the electrode surface. A bare GC electrode (a) and electrodes modified with PCA@MWCNT (b) and PCA@MWCNT-Ni(OH)$_2$ (c) were tested. For all materials, two areas changed depending on the frequency range; a small semicircle was seen in each high-frequency region and a line in each low-frequency region [23]. The experimental data were modeled using an equivalent Randles circuit (R_{ct}), presented in the inset of Figure 4B. The electron transfer resistance for the bare electrode was 444 Ω. The modification of the electrode with the use of the PCA@MWCNT hybrid material resulted in a decrease in the resistance to 13.9 Ω, confirming the electrochemical potential of the hybrid material. Electrodecoration with Ni(OH)$_2$ resulted in an R_{ct} value of 12.5 Ω. This indicates that the electrodeposition of nickel hydroxide facilitated the charge transfer

kinetics at the electrode, leading to the conclusion that the modification of the electrode with the use of the hybrid material PCA@MWCNT-Ni(OH)$_2$ enabled the achievement of electrochemical properties that make it suitable for electrocatalytic applications [22,23].
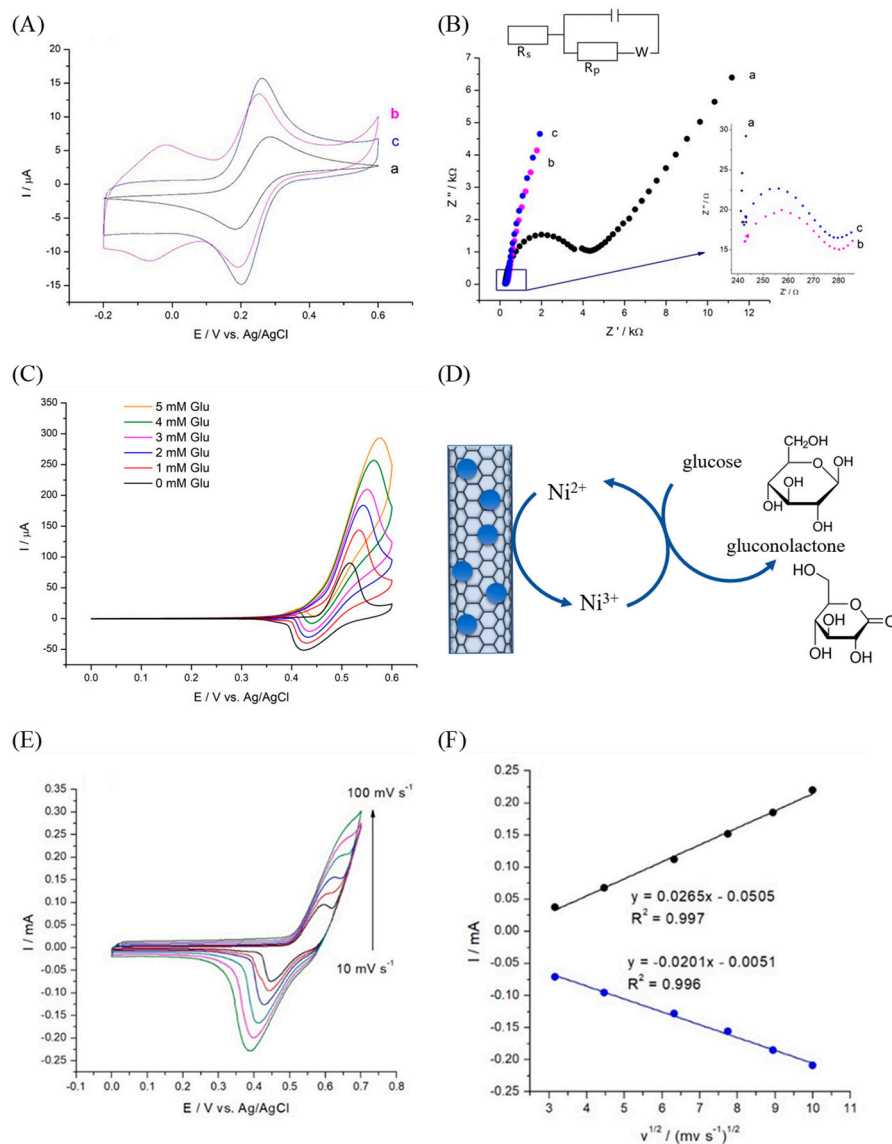
Figure 4. Cyclic voltammograms (**A**) and Nyquist plots (**B**) recorded in 0.1 M PBS, containing equimolar (1 mM) [Fe(CN)$_6$]$^{3-/4-}$ with the bare electrode (a), GC/PCA@MWCNT (b) and GC/PCA@MWCNT-Ni(OH)$_2$ (c). CVs of GC/PCA@MWCNT-Ni(OH)$_2$ in 0.1 M NaOH, with incremental concentrations of glucose from 0 mM to 5 mM. Scan rate: 10 mV s^{-1} (**C**). Schematic oxidation of glucose using Ni(OH)$_2$ (**D**). CVs of GC/PCA@MWCNT-Ni(OH)$_2$ with 1 mM of glucose in 0.1 M NaOH at different scan rates (1–100 mV s^{-1}) in 0.1 M NaOH (**E**). Relationship between peak current and square root of scan rate (**F**).

3.4. Glucose Electrocatalysis at GC/PCA@MWCNT-Ni(OH)$_2$

The CVs of GC/PCA@MWCNT-Ni(OH)$_2$, recorded in the presence of various glucose concentrations, are displayed in Figure 4C. It can be seen that the electrocatalytic oxidation of glucose was manifested by an increased anodic peak current at a potential close to that of the NiOOH/Ni(OH)$_2$ redox couple. The well-pronounced catalytic effect of the NiOOH/Ni(OH)$_2$ nanoparticles toward glucose could be observed when the redox response was compared with that of GC/MWCNT or GC/PCA@MWCNT. According to Figure S3, no redox signals from glucose oxidation were detected in the

case of GC/MWCNT or GC/PCA@MWCNT. These results suggest the suitability of the GC/PCA@MWCNT-Ni(OH)$_2$ hybrid electrode for glucose determination. Moreover, the shift of the oxidation peak relative to the positive potentials observed when the glucose concentration increased may have resulted from the limitation of the kinetics of the redox processes involved.

The electrode's catalytic mechanism is depicted in Figure 4D. The electrogenerated NiOOH oxidized glucose to gluconolactone in an alkaline solution, and simultaneously, the reduction of NiOOH to Ni(OH)$_2$ occurred, resulting in an increase in the oxidation peak current and a decrease in the reduction peak current in the reverse scan. The reaction mechanism of the electrochemical glucose oxidation can be summarized as follows [24]:

$$Ni(OH)_2 + OH^- \rightarrow NiOOH + H_2O + e^- \tag{4}$$

$$NiOOH + glucose \rightarrow Ni(OH)_2 + glucolactone \tag{5}$$
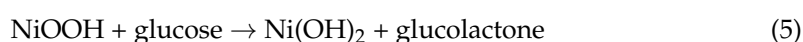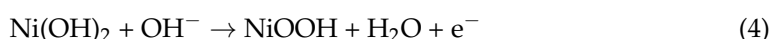
3.5. Optimization of PCA@MWCNT-Ni(OH)$_2$ Synthesis for Glucose Oxidation

The amount of Ni(OH)$_2$ on the PCA@MWCNT surface could be moderated using different concentrations of the Ni^{2+} precursor and different accumulation times. The loading of the Ni(OH)$_2$ catalyst was a crucial factor that determined the electrocatalytic efficiency in glucose oxidation. Hence, in the first stage, the effect of the time of adsorption (accumulation) of nickel was investigated, and the results are presented in Figure S4A,B. A quantity of 50 mM of NiSO$_4$ was used in these experiments. As shown, the charge measured under the anodic peak increased rapidly, up to an adsorption time of 2 min, and after this time, the redox signal formed a plateau, suggesting that adsorption equilibrium was achieved after 2 min. Subsequently, the effect of the Ni^{2+} concentration was studied by immersing the electrode in NiSO$_4$ solutions at various concentrations, from 10 to 500 mM, for 2 min (Figure S4C,D). The charge of the anodic peak increased significantly as the Ni^{2+} concentration increased from 10 to 100 mM. However, for higher Ni^{2+} concentrations, the redox response began to level out. To verify the optimum loading of nickel, the resultant electrodes were tested in the presence of glucose. The results showed that the highest catalytic current (expressed as I$_{glucose}$−I$_{background}$) was observed for an electrode prepared using 100 mM NiSO$_4$ (2 min of accumulation) (Figure S4E).

To determine the active surface areas for the bare GC and the modified electrodes, the cyclic voltammograms in 1 mM [Fe(CN)$_6$]$^{3-/4-}$ were recorded, as shown in Figure 5.

The current response increased both with the addition of the PCA@MWCNT and after the electrochemical deposition of the Ni(OH)$_2$ nanoparticles. The Randles–Ševčík equation was used to calculate the active surface area [25]:

$$Ip = 2.69 \cdot 10^5 \cdot A \cdot D^{1/2} \cdot n^{3/2} \cdot c \cdot v^{1/2} \tag{6}$$

where A is the effective electrode surface area (cm^2), Ip is the peak current (A), v$^{1/2}$ is the square root of the scan rate (V s^{-1}), D is the diffusion coefficient ($7.6 \cdot 10^{-6}$ cm^2 s^{-1}), *n* is the number of electrons (*n* = 1), and c is the concentration (mol cm^{-3}) [8,26].

The calculated electroactive surface area for the unmodified GC electrode was 0.028 cm^2. Modification with the use of the PCA@MWCNT nanomaterials led to a more than tenfold increase in the active surface. The electroactive surface areas for the GC/PCA@MWCNT and the GC/PCA@MWCNT-Ni(OH)$_2$ were calculated as 0.304 and 0.368 cm^2, respectively. Additionally, the active surface increased with the formation of Ni(OH)$_2$ particles, which were used as an electrocatalytic material for glucose oxidation.

For comparison, the electroactive surface area of a GC electrode modified with the GO/GPE material was 0.112 cm^2 [27]. Values of 0.144 cm^2 and 0.123 cm^2 of electroactive surface area were obtained for CuAlO$_2$ [28,29] and PtNPs [29], respectively.

To evaluate the kinetics of the glucose oxidation reaction in 0.1 M NaOH, the constructed GC/PCA@MWCNT-Ni(OH)$_2$ electrode was tested using cyclic voltammetry at

various scanning rates ranging from 10 to 100 mV s^{-1}. Figure 4E shows the CV plot of the electrode in the presence of 1 mM of glucose solution. As the scanning speed increases, the peak anode current increases and shifts slightly. As shown in Figure 4F, the anodic and cathodic current were plotted against the square root of the index scan, which gave linear relations with correlation coefficients (R^2) of 0.997 and 0.996, respectively, indicating that the proposed sensor oxidizes glucose in a diffusion-controlled process [30,31].
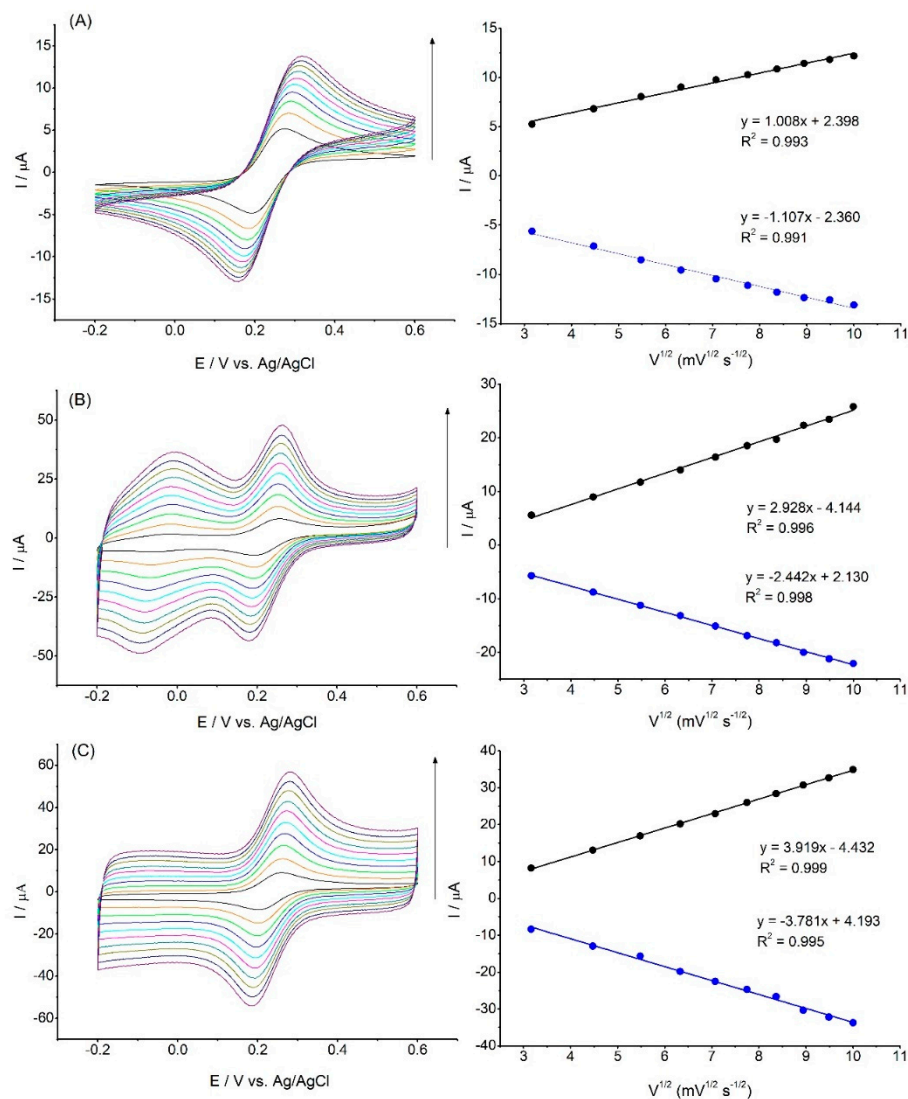

Figure 5. CV curves of GC (**A**), GC/PCA@MWCT (**B**), and GC/PCA@MWCNT-Ni(OH)$_2$ (**C**) at different scan rates (10–100 mV s^{-1}) in the presence of 1 mM of [Fe(CN)$_6$]$^{3-/4-}$ in 0.1 M PBS (pH: 7.4), as well as the calibration plot of peak current vs. square root of the scan rate.

3.6. Glucose Detection at GC/PCA@MWCNT-Ni(OH)$_2$

The amperometric responses of GC/PCA@MWCNT-Ni(OH)$_2$ (at a constant potential of +0.5 V) in 0.1 M of NaOH after the additions of different concentrations of glucose are shown in Figure 6A. The potential of 0.5 V used in the measurements is lower than those used in the cases of other nickel-based sensors, which can be considered an advantage of this system [32–34].
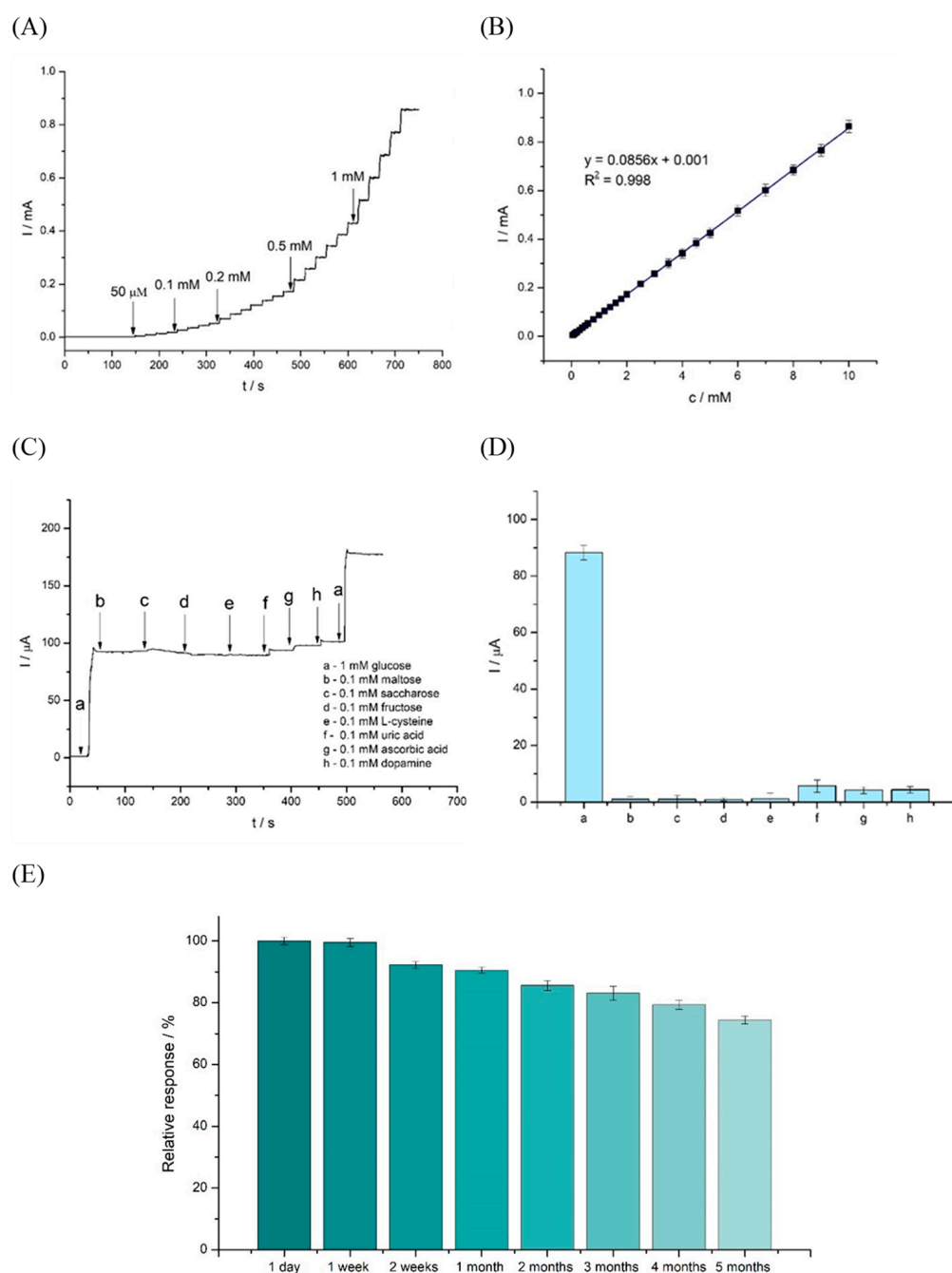
(A)

(B)

(C)

(D)

(E)

Figure 6. Amperometric response of a GC/PCA@MWCNT-Ni(OH)$_2$ electrode to successive additions of glucose at +0.5 V (**A**). The corresponding calibration curve (**B**). Amperometric responses of the GC/PCA@MWCNT-Ni(OH)$_2$ electrode under stirring conditions with the addition of 1 mM of glucose (a) and subsequent additions of 0.1 M maltose (b), 1 mM of saccharose (c), 0.1 mM of fructose (d), 0.1 mM of L-cysteine (e), 0.1 mM of uric acid (f), 0.1 mM of ascorbic acid (g), and 0.1 mM of dopamine (h) in 0.1 M NaOH solution at +0.5 V (**C**). The average sensor response in the presence of interferents ($n = 3$) (**D**). Stability over time of the proposed PCA@MWCNT-Ni(OH)$_2$ sensor for glucose determination: up to five months ($n = 3$) (**E**).

The current increased linearly and proportionally with increasing glucose levels (from 50 μM to 1 mM). The calibration plot of the glucose versus the current is shown in Figure 6B. The system exhibited high linearity in the range of 50 μM to 10 mM of glucose. In addition, the detection limit was determined to be 0.29 μM and the sensitivity of the sensor to be

232.7 μA mM^{-1} cm^{-2}. The analytical performance of the GC/PCA@MWCNT-Ni(OH)$_2$ sensor is compared with the published data for other glucose sensors in Table 1.

Table 1. Comparison of the present MWCNT@PCA-Ni(OH)$_2$ electrode to different non-enzymatic glucose sensors.

Electrode	Sensitivity /μA mM^{-1} cm^{-2}	LOD /μM	Linear Range /mM	Ref.
NiNP/SMWNTs	1438.0	0.50	0.001–0.1	[7]
NiO–MWCNTs/CPE	122.1	31.0	0.0–9.0	[35]
NiO-MWCNTs	436.0	160.0	0.2–1.2	[36]
Ti/TiO$_2$ NTA/Ni	200.0	4.0	0.1–1.7	[37]
Ni(OH)$_2$/ERGO–MWNT/GCE	2042.0	2.70	0.01–1.5	[38]
Ni(OH)$_2$/PU	2845.4	0.32	0.01–2.06	[39]
Ni(OH)$_2$-CNT-Nafion/GCE	238.5	0.50	0.1–1.1	[40]
NiO-OMC/GCE	834.8	0.65	0.002–1.0	[41]
CNT/Ni NAs	1381.0	1.0	0.5–10.0	[42]
PCA@MWCNT-Ni(OH)$_2$	**232.7**	**0.29**	**0.05–10.0**	**This work**

Amperometric experiments were also performed under static conditions. These tests were carried out at a constant potential of +0.5 V. A stabilized current value was obtained for the system after 30 s from the start of the measurements. The system was used to test glucose additions ranging from 0.1 to 10 mM (Figure S5A). Based on the curve fitted to the plot (Figure S5B), the sensitivity and the detection limit were determined to be 256.48 μA mM^{-1} cm^{-2} and 0.72 μM, respectively. The proposed non-enzymatic glucose sensor achieved a lower limit of detection (LOD) than reported enzymatic glucose sensors [43–45].

3.7. Interference Study

The presence of many interfering compounds is unavoidable in the detection environments of real applications; hence, resistance to these interfering substances is critical for glucose detection [46]. However, due to their higher electron transfer rates, these interfering species can yield oxidation currents comparable with that of glucose. It is envisaged that MWCNT@PCA-Ni(OH)$_2$-modified electrodes with large active surface areas will favor a kinetically regulated sluggish reaction (glucose oxidation) over diffusion-controlled reactions (the oxidations of interfering species) [7].

To verify the effects of interferents, the amperometric response of the modified MWCNT@PCA-Ni(OH)$_2$ electrode was tested with an applied potential of 0.5 V in 0.1 M NaOH solution (Figure 6C). In this experiment, 1 mM of glucose, 0.1 mM of maltose, 0.1 mM of saccharose, 0.1 mM of fructose, 0.1 mM of uric acid, 0.1 mM of ascorbic acid, and 0.1 mM of dopamine were added. As shown by the response curve in Figure 6D, a relatively high glucose signal was obtained compared with those of the interferents. The relative responses of the compounds compared with that of glucose ranged from 7.1% for fructose and 6.4% for maltose to 3% for saccharose. These results indicate that the MWCNT@PCA-Ni(OH)$_2$ electrode has good selectivity for glucose oxidation. The signals resulting from the presence of interfering agents were lower than those in the case of an NiO/GCE material, for example; the reasons for this include lower applied potential [47].

The influences of the analyzed interferents were also investigated in static conditions. Interferent solutions (0.1 mM) were assessed in the presence and absence of 1 mM of glucose to determine the interference effect. The influences of these compounds on the current responses of the produced sensor are shown in Figure S6A–H. Only slight changes in the response were produced by the interferents compared to the solution with glucose alone: 1.38% for sucrose, 3.27% for maltose, 5.58% for fructose, and 0.01% for dopamine (Figure S6I).

3.8. Stability, Reproducibility, and Repeatability

The stability of a sensor over time is critical for its practical implementation. External factors such as temperature, pH, and humidity affect electrodes during detection. The electrode's stability over time, in particular, has a direct impact on its service life and the cost of measurements [46]. Figure 6E shows that the GC/PCA@MWCNT-Ni(OH)$_2$ electrode retained 93.5% of its relative response after one month and 74.4% after 5 months of storage at 4 °C, indicating good long-term stability. Between months 4 and 5, there was a drop in the relative response from 79.4% to 74.4%. During the glucose oxidation process, reaction intermediates can be adsorbed onto the electrode surface. These adsorbed species may block active sites on the electrode, making it less effective in catalyzing the glucose oxidation reaction over time.

There are few data in the literature on the long-term stability of non-enzymatic sensors. This is a very important feature that determines the future application potential of such sensors. For example, Gong et al. investigated the stability of an Ni/Cu/BDD system over 30 days, obtaining 93.3% storage stability [46]. In comparison, Zeng et al. reported that an MWCNT-Ni-S nanomaterial retained 88.0% of its initial activity after just 18 days [48]. Table 2 shows a comparison of the stability of the sensor studied here with other Ni-based sensors.

Table 2. Comparison of the sensing performance of the PCA@MWCNT-Ni(OH)$_2$ electrode with other reported Ni nanostructure electrodes.

Glucose Sensor	Retained Activity (%)	Storage Time (Days)	References
Ni/Cu/BDD	93.3	30	[46]
MWCNT-Ni-S	88.0	18	[49]
Ni-NPs/TiO$_2$ nanotubes	80.3	20	[24]
NiO-APTS@SBA/CNT	95.0	24	[48]
Ni/Cu/MWCNT	90.0	30	[6]
MWCNT@PCA-Ni(OH)$_2$	**74.4**	**150**	**This work**

The stability of the proposed GC/PCA@MWCNT-Ni(OH)$_2$ electrode in the electrochemical process was studied by performing consecutive cycling in a potential range of 0 to 0.6 V for 200 cycles in a 0.1 M NaOH solution containing 1 mM of glucose (Figure S7A). As shown in the graph, after 200 scans, the system retained 90.1% of its initial response. The stability of the electrode was also tested in amperometric mode in the presence of 1 mM of glucose (Figure S7B). The electrode's initial current value decreased by 12% after 6000 s.

Other important parameters for non-enzymatic glucose sensors include reproducibility and repeatability. To test reproducibility, eight GC/PCA@MWCNT-Ni(OH)$_2$ electrodes were freshly obtained using the same process, and 1 mM of glucose was oxidized using these electrodes at a constant voltage of +0.5 V. A satisfactory relative standard deviation of 2.2% was obtained, as shown in Figure S8A. Cyclic voltammetry was then used to evaluate the repeatability of a single GC/PCA@MWCNT-Ni(OH)$_2$ electrode in the detection of 1 mM of glucose (eight measurements), giving a relative standard deviation (RSD) of 2.1% (Figure S8B). For comparison, the RSD reported for Ni(OH)$_2$-CNT-PVDF was 2.5% [50], while for Ni(OH)$_2$ deposited on sulfur-doped carbon (SDCN), it was 3.2% [51].

3.9. Real Samples

To evaluate its suitability for practical application, the MWCNT@PCA-Ni(OH)$_2$ sensor was used to determine the glucose in human serum and human blood samples. As shown in Table 3, recovery of glucose was measured by adding glucose to solutions containing serum samples using a standard addition procedure. The proposed sensor presented recoveries in the range of 96.3–98.2%.

Table 3. Detection of glucose in human serum and human blood samples with the GC/PCA@MWCNT-Ni(OH)$_2$ sensor ($n = 3$).

Sample	Glucose Concentration/mM	GC/MWCNT@PCA-Ni(OH)$_2$	
		Find/mM	Recovery/%
Human Serum	2.4	2.31 ± 0.05	96.3 ± 2.1
	6.6	6.44 ± 0.08	97.6 ± 1.2
	8.5	8.35 ± 0.12	98.2 ± 1.4
Human Blood	3.2	3.08 ± 0.06	96.4 ± 1.9
	6.3	5.88 ± 0.07	93.3 ± 1.1
	14.7	14.35 ± 0.15	97.6 ± 1.0

The electrode was also tested on human blood solutions. Three different glucose concentrations (3.2, 6.3, and 14.7 mM of glucose) were tested. The recoveries ranged from 93.3% to 97.6% for the detection of glucose in human blood. These results confirm that the non-enzymatic sensor can be used to determine glucose concentrations in biological samples with real glucose concentrations.

4. Conclusions

In this study, electroactive Ni(OH)$_2$ was successfully electrodeposited on the surface of a chemically synthesized PCA@MWCNT material. The single-step electrochemical deposition process described in this work allowed the fabrication of a sensor containing Ni(OH)$_2$ nanoparticles, which exhibited excellent performance in the detection of glucose, with high sensitivity and a low detection limit. The non-enzymatic sensor also demonstrated good stability over a time period of 5 months from its construction. In addition, the sensor was used to detect glucose in real solutions: human blood and human serum. The results have confirmed that the proposed sensor has the potential for application in non-enzymatic glucose detection.

Supplementary Materials: The following supporting information can be downloaded at: https://www.mdpi.com/article/10.3390/chemosensors11080452/s1, Figure S1: 2D AFM image (A) and surface profile analysis (B) of PCA@MWCNT-Ni(OH)$_2$; Figure S2: EDS mapping spectrum of PCA@MWCNT-Ni(OH)$_2$ (A) and SEM micrographs of elemental carbon (B), oxygen (C), and nickel (D); Table S1: EDS analysis results for PCA@MWCNT-Ni(OH)$_2$ material; Figure S3: CVs of 0.1 M NaOH solution at GC/MWCNT (A), GC/PCA@MWCNT (B), GC/PCA@MWCNT-Ni(OH)$_2$ (C) in the absence (a) and presence (b) of 1 mM glucose at 10 mV s^{-1}; Figure S4: Change in GC/PCA@MWCNT-Ni(OH)$_2$ redox response depending on the complexation time of NiSO$_4$ used in the fabrication of GC/PCA@MWCNT-Ni(OH)$_2$ (concentration of NiSO$_4$ was 50 mM) (A). Relationship between anodic peak charge and time of accumulation (B). Change in GC/PCA@MWCNT-Ni(OH)$_2$ redox response depending on the concentration of NiSO$_4$ used in the fabrication of GC/PCA@MWCNT-Ni(OH)$_2$ (time of accumulation was 2 min) (C). Relationship between anodic peak charge and NiSO$_4$ concentration (D). Value of $I_{glucose} - I_{background}$ recorded at GC/PCA@MWCNT-Ni(OH)$_2$ prepared using various NiSO$_4$ concentrations (E); Figure S5: Chronoamperometric responses of GC/PCA@MWCNT-Ni(OH)2 for various glucose concentrations (100 μM $-$ 10 mM) in 0.1 M NaOH at +0.5 V (A); the corresponding calibration curve of current response vs. glucose concentration (B) ($n = 3$); Figure S6: GC/PCA@MWCNT-Ni(OH)$_2$ sensor's amperometric response to 1 mM glucose (A) and individual interferents (0.1 mM): maltose (B), saccharose (C), fructose (D), uric acid (E), ascorbic acid (F), L-cysteine (G), dopamine (H), in the absence and presence of 1 mM glucose in 0.1 M NaOH solution at +0.5 V, (I) comparison of the relative response for the tested interferents against glucose. Figure S7: CV curves recorded in 1 mM glucose at the first measurement (a) and after 200 consecutive measurements (b) (A); chronoamperometric response of the GC/PCA@MWCNT-Ni(OH)$_2$ electrode after 6000 s at +0.5 V (B). Figure S8: Reproducibility of eight electrodes for the detection of 1 mM glucose (A); repeatability of a single electrode for detection in eight samples containing 1 mM glucose (B).

References

1. Liu, D.; Wang, J.; Wu, L.; Huang, Y.; Zhang, Y.; Zhu, M.; Wang, Y.; Zhu, Z.; Yang, C. Trends in miniaturized biosensors for point-of-care testing. *Trends Anal. Chem.* **2020**, *122*, 115701. [CrossRef]
2. Jędrzak, A.; Kuznowicz, M.; Rębiś, T.; Jesionowski, T. Portable glucose biosensor based on polynorepinephrine@magnetite nanomaterial integrated with a smartphone analyzer for point-of-care application. *Bioelectrochemistry* **2022**, *145*, 108071. [CrossRef]
3. Panda, P.; Pal, K.; Chakroborty, S. Smart advancements of key challenges in graphene-assembly glucose sensor technologies: A mini review. *Mater. Lett.* **2021**, *303*, 130508. [CrossRef]
4. Huang, C.; Hao, Z.; Qi, T.; Pan, Y.; Zhao, X. An integrated flexible and reusable graphene field effect transistor nanosensor for monitoring glucose. *J. Mater.* **2020**, *6*, 308–314. [CrossRef]
5. Zhang, Q.; Luo, Q.; Qin, Q.; Liu, L.; Wu, Z.; Shen, B.; Hu, W. Self-Assembly of Graphene-Encapsulated Cu Composites for Nonenzymatic Glucose Sensing. *ACS Omega* **2018**, *3*, 3420–3428. [CrossRef] [PubMed]
6. Yi, W.; Liu, J.; Chen, H.; Gao, Y.; Li, H. Copper/nickel nanoparticle decorated carbon nanotubes for nonenzymatic glucose biosensor. *J. Solid. State Electrochem.* **2015**, *19*, 1511–1521. [CrossRef]
7. Nie, H.; Yao, Z.; Zhou, X.; Yang, Z.; Huang, S. Nonenzymatic electrochemical detection of glucose using well-distributed nickel nanoparticles on straight multi-walled carbon nanotubes. *Biosens. Bioelectron.* **2011**, *30*, 28–34. [CrossRef]
8. Kuznowicz, M.; Rębiś, T.; Jędrzak, A.; Nowaczyk, G.; Szybowicz, M.; Jesionowski, T. Glucose determination using amperometric non-enzymatic sensor based on electroactive poly(caffeic acid)@MWCNT decorated with CuO nanoparticles. *Microchim. Acta* **2022**, *189*, 159. [CrossRef]
9. Ahmad, R.; Tripathy, N.; Ahn, M.S.; Bhat, K.S.; Mahmoudi, T.; Wang, Y.; Yoo, J.Y.; Kwon, D.W.; Yang, H.Y.; Hahn, Y.B. Highly Efficient Non-Enzymatic Glucose Sensor Based on CuO Modified Vertically-Grown ZnO Nanorods on Electrode. *Sci. Rep.* **2017**, *7*, 5715. [CrossRef]
10. Pal, N.; Banerjee, S.; Bhaumik, A. A facile route for the syntheses of $Ni(OH)_2$ and NiO nanostructures as potential candidates for non-enzymatic glucose sensor. *J. Colloid. Interface Sci.* **2018**, *516*, 121–127. [CrossRef]
11. Zhan, B.; Liu, C.; Chen, H.; Shi, H.; Wang, L.; Chen, P.; Huang, W.; Dong, X. Free-standing electrochemical electrode based on $Ni(OH)_2$/3D graphene foam for nonenzymatic glucose detection. *Nanoscale* **2014**, *6*, 7424–7429. [CrossRef]
12. Liu, X.; Yu, L. Influence of nanosized $Ni(OH)_2$ addition on the electrochemical performance of nickel hydroxide electrode. *J. Power Sources* **2004**, *128*, 326–330. [CrossRef]
13. Monahan, J.; Wilker, J.J. Specificity of metal ion cross-linking in marine mussel adhesives. *Chem. Commun.* **2003**, *14*, 1672–1673. [CrossRef]
14. Rębiś, T.; Kuznowicz, M.; Jędrzak, A.; Milczarek, G.; Jesionowski, T. Design and fabrication of low potential NADH-sensor based on poly(caffeic acid)@multi-walled carbon nanotubes. *Electrochim. Acta.* **2021**, *386*, 138384. [CrossRef]
15. Liu, Y.; Wang, R.; Yan, X. Synergistic effect between ultra-small nickel hydroxide nanoparticles and reduced graphene oxide sheets for the application in high-performance asymmetric supercapacitor. *Sci. Rep.* **2015**, *5*, 11095. [CrossRef]
16. Salunkhe, R.R.; Lin, J.; Malgras, V.; Dou, S.X.; Kim, J.H.; Yamauchi, Y. Large-scale synthesis of coaxial carbon nanotube/$Ni(OH)_2$ composites for asymmetric supercapacitor application. *Nano Energy* **2015**, *11*, 211–218. [CrossRef]
17. Subramanian, A.S.; Tey, J.N.; Zhang, L.; Ng, B.H.; Roy, S.; Wei, J.; Hu, X.M. Synergistic bond strengthening in epoxy adhesives using polydopamine/MWCNT hybrids. *Polymer* **2016**, *82*, 285–294. [CrossRef]
18. Zhang, Y.; Dong, K.; Liu, Z.; Wang, H.; Ma, S.; Zhang, A.; Li, M.; Yu, L.; Li, Y. Sulfurized hematite for photo-Fenton catalysis. *Prog. Nat. Sci.* **2018**, *27*, 443–451. [CrossRef]
19. Zhou, Y.; Li, J.; Wang, S.; Zhang, J.; Kang, Z. From MOF membrane to 3D electrode: A new approach toward an electrochemical non-enzymatic glucose biosensor. *J. Mater. Sci.* **2017**, *52*, 12089–12097. [CrossRef]
20. Duc Chinh, V.; Speranza, G.; Migliaresi, C.; Van Chuc, N.; Minh Tan, V.; Phuong, N.T. Synthesis of Gold Nanoparticles Decorated with Multiwalled Carbon Nanotubes (Au-MWCNTs) via Cysteaminium Chloride Functionalization. *Sci. Rep.* **2019**, *9*, 5667. [CrossRef] [PubMed]
21. Dubal, D.P.; Gund, G.S.; Lokhande, C.D.; Holze, R. Decoration of spongelike $Ni(OH)_2$ nanoparticles onto MWCNTs using an easily manipulated chemical protocol for supercapacitors. *ACS Appl. Mater. Interfaces* **2013**, *5*, 2446–2454. [CrossRef] [PubMed]
22. Wu, Y.; Yang, X.; Liu, S.; Xing, Y.; Peng, J.; Peng, Y.; Ni, G.; Jin, X. One-step synthesis of $Ni(OH)_2$/MWCNT nanocomposites for constructing a nonenzymatic hydroquinone/O_2 fuel cell. *RSC Adv.* **2020**, *10*, 39447–39454. [CrossRef]

23. Martínez-Sánchez, C.; Regmi, C.; Lee, S.W.; Rodríguez-González, V. Effects of Ce Doping on the Photocatalytic and Electrochemical Performance of Nickel Hydroxide Nanostructures. *Top. Catal.* **2021**, *64*, 73–83. [CrossRef]

24. Yu, S.; Peng, X.; Cao, G.; Zhou, M.; Qiao, L.; Yao, J.; He, H. Ni nanoparticles decorated titania nanotube arrays as efficient nonenzymatic glucose sensor. *Electrochim. Acta.* **2012**, *76*, 512–517. [CrossRef]

25. Holze, R. *Book Review: Electrochemical Methods. Fundamentals and Applications*, 2nd ed.; Angewandte Chemie-International, Ed.; Wiley: Hoboken, NJ, USA, 2022; Volume 41, pp. 655–657.

26. Bilal, S.; Ullah, W.; Ali Shah, A. Polyaniline@CuNi nanocomposite: A highly selective, stable and efficient electrode material for binder free non-enzymatic glucose sensor. *Electrochim. Acta.* **2018**, *284*, 382–391. [CrossRef]

27. Baig, N.; Kawde, A.N.; Ibrahim, M. Efficient ionic medium supported reduced graphene oxide-based sensor for selective sensing of dopamine. *Mater. Adv.* **2022**, *4*, 783–793. [CrossRef]

28. Ahmed, J.; Mao, Y. Delafossite $CuAlO_2$ nanoparticles with electrocatalytic activity toward oxygen and hydrogen evolution reactions. *ACS Symp. Ser.* **2015**, *1213*, 57–72.

29. Baron, R.; Campbell, F.W.; Streeter, I.; Xiao, L.; Compton, R.G. Facile method for the construction of random nanoparticle arrays on a carbon support for the development of well-defined catalytic surfaces. *Int. J. Electrochem. Sci.* **2008**, *3*, 556–565. [CrossRef]

30. Kiani, M.A.; Tehrani, M.A.; Sayahi, H. Reusable and robust high sensitive non-enzymatic glucose sensor based on $Ni(OH)_2$ nanoparticles. *Anal. Chim. Acta* **2014**, *839*, 26–33. [CrossRef]

31. Jędrzak, A.; Rębiś, T.; Kuznowicz, M.; Jesionowski, T. Bio-inspired magnetite/lignin/polydopamine-glucose oxidase biosensing nanoplatform. From synthesis, via sensing assays to comparison with others glucose testing techniques. *Int. J. Biol. Macromol.* **2019**, *127*, 677–682. [CrossRef]

32. Zhang, X.; Zhang, Z.; Liao, Q.; Liu, S.; Kang, Z.; Zhang, Y. Nonenzymatic glucose sensor based on in situ reduction of Ni/NiO-graphene nanocomposite. *Sensors* **2016**, *16*, 1791. [CrossRef]

33. Zhong, X.; He, Z.; Chen, H.; Chen, Y. Enhancing the non-enzymatic glucose detection performance of $Ni(OH)_2$ nanosheets via defect engineering. *Surf. Interfaces* **2021**, *25*, 101234. [CrossRef]

34. Radwan, A.B.; Paramparambath, S.; Cabibihan, J.J.; Al-Ali, A.K.; Kasak, P.; Shakoor, R.A.; Malik, R.A.; Mansour, S.A.; Sadasivuni, K.K. Superior non-invasive glucose sensor using bimetallic CuNi nanospecies coated mesoporous carbon. *Biosensors* **2021**, *11*, 463. [CrossRef] [PubMed]

35. Prasad, R.; Bhat, B.R. Multi-wall carbon nanotube-NiO nanoparticle composite as enzyme-free electrochemical glucose sensor. *Sens. Actuators B Chem.* **2015**, *220*, 81–90. [CrossRef]

36. Shamsipur, M.; Najafi, M.; Hosseini, M.R.M. Highly improved electrooxidation of glucose at a nickel(II) oxide/multi-walled carbon nanotube modified glassy carbon electrode. *Bioelectrochemistry* **2010**, *77*, 120–124. [CrossRef]

37. Wang, C.; Yin, L.; Zhang, L.; Gao, R. Ti/TiO_2 nanotube array/Ni composite electrodes for nonenzymatic amperometric glucose sensing. *J. Phys. Chem. C* **2010**, *114*, 4408–4413. [CrossRef]

38. Gao, W.; Tjiu, W.W.; Wei, J.; Liu, T. Highly sensitive nonenzymatic glucose and H_2O_2 sensor based on $Ni(OH)_2$/electroreduced graphene oxide-Multiwalled carbon nanotube film modified glass carbon electrode. *Talanta* **2014**, *120*, 484–490. [CrossRef] [PubMed]

39. Guo, S.; Zhang, C.; Yang, M.; Zhou, Y.; Bi, C.; Lv, Q.; Ma, N. A facile and sensitive electrochemical sensor for non-enzymatic glucose detection based on three-dimensional flexible polyurethane sponge decorated with nickel hydroxide. *Anal. Chim. Acta* **2020**, *1109*, 130–139. [CrossRef] [PubMed]

40. Yang, H.; Gao, G.; Teng, F.; Liu, W.; Chen, S.; Ge, Z. Nickel Hydroxide Nanoflowers for a Nonenzymatic Electrochemical Glucose Sensor. *J. Electrochem. Soc.* **2014**, *161*, B216–B219. [CrossRef]

41. Luo, L.; Li, F.; Zhu, L.; Ding, Y.; Zhang, Z.; Deng, D.; Lu, B. Nonenzymatic glucose sensor based on nickel(II)oxide/ordered mesoporous carbon modified glassy carbon electrode. *Colloids Surf. B Biointerfaces* **2013**, *102*, 307–311. [CrossRef]

42. Zhu, J.; Jiang, J.; Liu, J.; Ding, R.; Li, Y.; Ding, H.; Feng, Y.; Wei, G.; Huang, X. CNT-network modified Ni nanostructured arrays for high performance non-enzymatic glucose sensors. *RSC Adv.* **2011**, *1*, 1020–1025. [CrossRef]

43. Nien, P.C.; Tung, T.S.; Ho, K.C. Amperometric glucose biosensor based on entrapment of glucose oxidase in a poly(3,4-ethylenedioxythiophene) film. *Electroanalysis* **2006**, *18*, 1408–1415. [CrossRef]

44. Wu, B.; Xu, H.; Shi, Y.; Yao, Z.; Yu, J.; Zhou, H.; Li, Y.; Chen, Q.; Long, Y. Microelectrode glucose biosensor based on nanoporous platinum/graphene oxide nanostructure for rapid glucose detection of tomato and cucumber fruits. *Food Qual.* **2022**, *6*, fyab030. [CrossRef]

45. Palanisamy, S.; Cheemalapati, S.; Chen, S.M. Amperometric glucose biosensor based on glucose oxidase dispersed in multiwalled carbon nanotubes/graphene oxide hybrid biocomposite. *Mater. Sci. Eng. C* **2014**, *34*, 207–213. [CrossRef]

46. Gong, Z.; Hu, N.; Ye, W.; Zheng, K.; Li, C.; Ma, L.; Wei, Q.; Yu, Z.; Zhou, K.; Huang, N.; et al. High-performance non-enzymatic glucose sensor based on Ni/Cu/boron-doped diamond electrode. *J. Electroanal. Chem.* **2019**, *841*, 135–141. [CrossRef]

47. Jamal, M.; Chakrabarty, S.; Shao, H.; McNulty, D.; Yousuf, M.; Furukawa, H.; Khosla, A.; Razeeb, K. A non enzymatic glutamate sensor based on nickel oxide nanoparticle. *Microsyst. Technol.* **2018**, *24*, 217–4223. [CrossRef]

48. Baghayeri, M.; Sedrpoushan, A.; AMohammadi, M. Heidari, A non-enzymatic glucose sensor based on NiO nanoparticles/functionalized SBA 15/MWCNT-modified carbon paste electrode. *Ionics* **2017**, *23*, 1553–1562. [CrossRef]

49. Zeng, G.; Li, W.; Ci, S.; Jia, J.; Wen, Z. Highly Dispersed NiO Nanoparticles Decorating graphene Nanosheets for Non-enzymatic Glucose Sensor and Biofuel Cell. *Sci. Rep.* **2016**, *6*, 36454. [CrossRef]

50. Yan, X.; Guangwei, G.; Zhu, G.; Gao, J.; Ge, Z.; Yang, H. A Nonenzymatic Electrochemical Glucose Sensor Based on Ni(OH)$_2$-CNT-PVDF Composite and Its Application in Measuring Serum Glucose. *J. Electrochem. Soc.* **2014**, *161*, B106–B110.
51. Karikalan, N.; Velmurugan, M.; Chen, S.-M.; Karuppiah, C. Modern Approach to the Synthesis of Ni(OH)$_2$ Decorated Sulfur Doped Carbon Nanoparticles for the Nonenzymatic Glucose Sensor. *ACS Appl. Mater. Interfaces* **2016**, *8*, 22545–22553. [CrossRef]